ACS APPLIED ENERGY MATERIALS

www.acsaem.org Article

Triazatruxene-Based Ordered Porous Polymer: High Capacity CO_2, CH_4, and H_2 Capture, Heterogeneous Suzuki–Miyaura Catalytic Coupling, and Thermoelectric Properties

Ali Enis Sadak,*,‡ Erman Karakuş,*,‡ Yurii M. Chumakov, Nesibe A. Dogan, and Cafer T. Yavuz

Cite This: *ACS Appl. Energy Mater.* 2020, 3, 4983–4994 Read Online

ACCESS | Metrics & More | Article Recommendations | Supporting Information

ABSTRACT: A hypercrosslinked ultramicroporous and ordered organic polymer network was synthesized from a planar trimer indole building block called triazatruxene (TAT) through anhydrous $FeCl_3$ catalyzed Friedel–Crafts alkylation using methylal as a crosslinker. The polymer network is stable in a variety of chemicals and thermally durable. The hypercrosslinked network TATHCP shows a high BET (Brunauer–Emmet–Teller) specific surface area of 997 m^2 g^{-1} with CO_2 uptake capacity of 12.55 wt % at 273 K, 1.1 bar. Gas selectivities of 38.4 for CO_2/N_2, 7.8 for CO_2/CH_4, 40.6 for CO_2/O_2, and 32.1 for CO_2/CO were achieved through IAST calculation. The PXRD analysis has revealed that TATHCP has a fully eclipsed structure in full agreement with Pawley refinement. The ordered 2D layers provide anisotropy that could be used in catalysis and thermoelectric measurements. After loading with Pd(II), TATHCP-Pd showed high catalytic activity in Suzuki–Miyaura cross coupling reaction with a wide range of reagents and excellent reaction yields of 90–98% with good recyclability. The structure of TATHCP-Pd was found to have two independent molecules of $Pd(OAc)_2$ in the asymmetric unit cell which are arranged between two TATHCP layers. Thermoelectric properties of TATHCP showed a high Seebeck coefficient and ZT, a first and promising example in HCPs with applications in all-organic thermal energy recovery devices.

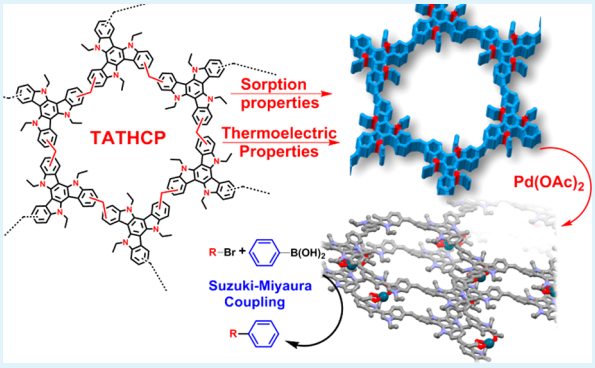

KEYWORDS: *triazatruxene, ordered porous polymer, hypercrosslinking, ultramicroporous, Friedel–Crafts, Pawley refinement, Suzuki–Miyaura cross coupling, thermoelectric, Seebeck coefficient*

INTRODUCTION

Porous networks with high surface areas have received considerable scientific interest due to their potential in applications like separations,[1,2] catalysis,[3,4] and gas sorptions.[5−9] Over the last few decades, a series of new porous materials such as covalent organic frameworks (COFs),[10,11] metal organic frameworks (MOFs),[12] microporous organic polymers (MOPs),[13] and porous organic cages[14] have been introduced. MOPs, in particular, are of great interest because of their high surface areas, low structural densities, and exceptional chemical stabilities. Their application in heterogeneous catalysis and other emerging applications like thermoelectric materials, however, has not been as thorough as those for COFs and MOFs.[15,16]

Hypercrosslinked polymers (HCPs), a subclass of MOPs, were first synthesized by Davankov et al. in the early 1990s.[17] Although they were initially used for chromatography, their applicability in trapping organic vapors and removing impurities in liquid solutions showed great promise.[17−21] The hyper-cross-linking can be produced in several ways such as bottom-up integration of rigid building blocks or postsynthetic cross-linking of polymer chains. Regardless of the methods, the structure of the material does not deteriorate even after removal of the solvent, since a vast number of rigid crosslinking improves framework cohesion and lasting porosity. The easy and scalable production processes along with their inherently robust structures make HCPs good candidates for capturing carbon, separating gas mixtures, storing energy and catalysis. Although recent examples focused on gas separations, to the best of our knowledge, metal-coordinated catalytic activity of the ordered 2D layers has not been presented so far.

Triazatruxene (TAT) is a fully aromatic molecule with a planar C_3 symmetrical trimer structure of three indole molecules. At the same time, from a different perspective, the integration of three carbazole molecules around the same

Received: March 12, 2020
Accepted: April 20, 2020
Published: April 20, 2020

benzene molecule also forms a triazatruxene structure. There are a few studies in which carbazole structure is used as a core for gas storage and synthesis of metal coordinated HCP catalysts.[22−27] Having three functional heteroatoms at positions 5, 10, and 15 allows for a wide variety of reactions. TAT has recently gained interest due to its high degree of electron donation capability with π-conjugated structure.[28−30] High electron mobility was also recorded from TAT derivatives.[28] The incorporation of TAT molecule into complex structures has a great positive effect on thermal stability.[31,32] COF networks consisting of TAT monomers are found to be highly stable in many solvents and acidic environments.[33,34] The presence of nitrogen atoms containing unpaired electrons on the polymer increases the affinity of the polymer with the carbon dioxide molecule, resulting in a high capacity carbon dioxide capture.[35] Second, the material should provide ample coordination with its catalytic active sites. TAT's nitrogen atoms on pyrrole rings have a potential for incorporating metal ions.[36] All these properties inspired us to investigate the probability of using metal-ion-including TATHCP material in both catalysis and gas sorption experiments. In addition, because of the stacking order of 2D layers in TATHCP, we envisioned thermoelectric properties that rely on anisotropic, directional thermal conductivity in a perpendicular alignment with electrical conductivity.

In this work, we report for the first time the design, synthesis, gas uptake, catalytic applications, and thermoelectric properties of a highly porous, ordered triazatruxene HCP material using methylal as an external cross-linker.

EXPERIMENTAL SECTION

Materials. $POCl_3$ of 99% purity was purchased from Sigma-Aldrich. 2-Oxoindole of 97% purity was procured from Sigma-Aldrich. Methylal of ≥93.0 purity was purchased from Sigma-Aldrich. KOH of ≥85% purity was purchased from Merck. All materials were used as received, unless otherwise stated.

10,15-Dihydro-5H-diindolo[3,2-a:3′,2′-c]carbazole (Triazatruxene, 2). $POCl_3$ (16 g, 105 mmol) and 2-oxoindole (**1**; 2 g, 15 mmol) were added into a 50 mL round-bottomed flask and the reaction mixture was stirred at 100 °C for 8 h. The solution was cooled to room temperature, transferred into a 500 mL beaker containing crushed ice (250 mL), and neutralized by the addition of adequate amount of saturated KOH solution. The resulting brown colored precipitate was collected by filtration and the crude product (1.2 g) was purified by silica gel column chromatography by using 1:4 acetone/hexane as the eluent. After crystallization from 1:1 acetone/hexane, 10,15-dihydro-5*H*-diindolo[3,2-*a*:3′,2′-*c*]carbazole (**2**) was obtained (yield: 40%, 0.8 g).[37] Melting point: 393−394 °C. ^{1}H NMR (600 MHz, DMSO): δ 11.86 (bs, 3H), 8.67 (d, J = 7.6 Hz, 3H), 7.73 (d, J = 7.6 Hz, 3H), 7.40−7.32 (m, 6H). APT ^{13}C NMR (150 MHz, DMSO): δ 139.0, 134.2, 123.0, 122.7, 120.3, 119.5, 111.4, 101.0. IR (KBr, cm^{-1}): 3473, 3439, 3053, 3025, 2919, 2852, 1737, 1635, 1273, 729.

5,10,15-Triethyl-10,15-dihydro-5H-diindolo[3,2-a:3′,2′-c]carbazole (3). Triazatruxene (**2**; 1.85 g, 5.36 mmol) and KOH (4.51 g, 80.34 mmol, 15 equiv) were dissolved in 100 mL of anhydrous THF heated at 70 °C for 3.5 h. After the mixture was cooled to room temperature, bromoethane (2.33 g, 21.42 mmol, 4 equiv) was added to the mixture. The mixture was stirred magnetically at room temperature for 1 day. After the reaction was completed, the solvent was removed in vacuo. The crude product was dissolved in 200 mL of EtOAc and the organic phase was washed with water (3 × 100 mL) and dried over Na_2SO_4. The solvent was removed in vacuo. The crude product was purified on silica gel (25 g) column chromatography by using 1:4 CH_2Cl_2/hexane. After crystallization over 1:1 CH_2Cl_2/acetone, 5,10,15-triethyl-10,15-dihydro-5*H*-diindolo[3,2-*a*:3′,2′-*c*]-carbazole (**3**) was obtained (yield: 82%, 1.9 g). ^{1}H NMR (600 MHz, $CDCl_3$): δ, ppm 8.37 (d, J = 8.0 Hz, 3H), 7.68 (d, J = 8.0 Hz, 3H), 7.48 (t, J = 7.4 Hz, 3H), 7.37 (t, J = 7.4 Hz, 3H), 5.05 (t, J = 7.2 Hz, 6H), 1.64 (t, J = 7.2 Hz, 9H). ^{13}C NMR (150 MHz, $CDCl_3$): δ, ppm 143.4, 141.4, 126.2, 125.4, 124.1, 122.5, 113.0 105.9, 44.4, 18.2. IR (powder, cm^{-1}): 3045, 2970, 1555, 1480, 1320, 1233, 1098, 724. HRMS: m/z: calcd for ($C_{30}H_{27}N_3$) [M + H$^+$], 430.22385; found, 430.22868.

Synthesis of TATHCP. To the mixture of 5,10,15-triethyl-10,15-dihydro-5*H*-diindolo[3,2-*a*:3′,2′-*c*]carbazole (**3**) (0.500 g, 1.16 mmol) and methylal (0.266 g, 3.49 mmol, 3 equiv) in 20 mL of 1,2-dichloroethane, anhydrous $FeCl_3$ (0.566 g, 3.49 mmol, 3 equiv) was added at room temperature. The mixture was heated to 40 °C and stirred for 5 h then set to 80 °C and stirred under this temperature for 19 h under an inert (N_2) atmosphere. After 19 h, the reaction was stopped and cooled to room temperature. The solid product was filtered and repeatedly washed with methanol, distilled water, concentrated HCl, and methanol to eliminate the unreacted monomer and $FeCl_3$ until the filtrate was almost pale. After that the TATHCP was boiled for extra purification by Soxhlet extraction from methanol (50 mL) for 24 h. The product was dried in vacuum for 24 h at 80 °C to give brown-colored solid powder (yield: 551 mg, 92.5%). IR (powder, cm^{-1}): 2957, 1562, 1440, 1316, 1212, 1069, 792, 743.

Synthesis of TATHCP-Pd. To 10 mL of dichloromethane was added $Pd(OAc)_2$ (45 mg, 0.2 mmol), and the mixture was stirred until dissolved. The TATHCP (165 mg) was then added. The reaction mixture was stirred magnetically at room temperature for 24 h. The solid product was filtered and washed with boiling dichloromethane using Soxhlet extraction for 48 h. The product was dried in vacuum for 24 h at 80 °C to give TATHCP-Pd as a dark brown-colored solid powder (170 mg, 80% yield). The Pd content was found to be 4.12% by ICP analysis. IR (powder, cm^{-1}): 2958, 1573, 1446, 1376, 1322, 1220, 1079, 796, 776, 737.

General Process for TATHCP-Pd in Suzuki−Miyaura Coupling Reaction. In a general set of optimized Suzuki−Miyaura coupling reaction, catalytic activity test of TATHCP-Pd, in 4 mL of *p*-xylene there were added aryl halides (1.0 mmol), phenylboronic acid (1.5 mmol), potassium carbonate (2.0 mmol) and TATHCP-Pd (15 mg, 0.5 mol %) and 200 μL distilled water. The mixture was refluxed at 150 °C under nitrogen atmosphere and the progress of the reaction was controlled by thin layer chromatography (TLC). After the reaction was completed the mixture was vacuum filtered with G4 Buchner funnel and the solid was clean with CH_2Cl_2 (20 mL). The liquid phase was washed with water (20 mL) to remove base then dried over sodium sulfate and evaporated at 60 °C under vacuum to give the crude products. The yields were calculated from the ^{1}H NMR spectra based on aryl halides (Table 2).

Reusability of TATHCP-Pd Catalyst in Suzuki−Miyaura Reactions. In the catalyst recyclability test, in 4 mL of *p*-xylene there were added phenylboronic acid (1.5 mmol), potassium carbonate (2.0 mmol), *p*-nitrobromobenzene (1.0 mmol), and TATHCP-Pd (30 mg, 1.0 mol %) and 200 μL distilled water. After the end of each cycle, the TATHCP-Pd catalyst was isolated from reaction mixture by vacuum filtration and was reused in the next catalytic run (Table 3). Comprehensive experimental details are provided in the Supporting Information.

RESULTS AND DISCUSSION

Synthesis and Characterization. The "knitting" method is one of the easiest methods used in large scale synthesis of HCPs.[38] By using this method, a wide variety of hypercrosslinked polymer materials could be obtained from aromatic compounds which, otherwise, do not have traditional functional groups for polymerization.[39] Herein, we introduce a new hypercrosslinked polymer network, obtained through Friedel−Crafts crosslinking using methylal as an external linker and TAT; a planar, rigid nonfunctionalized heteroatomic aromatic building block (Figure 1a). As with most other reported HCPs,

https://dx.doi.org/10.1021/acsaem.0c00539
ACS Appl. Energy Mater. 2020, 3, 4983−4994

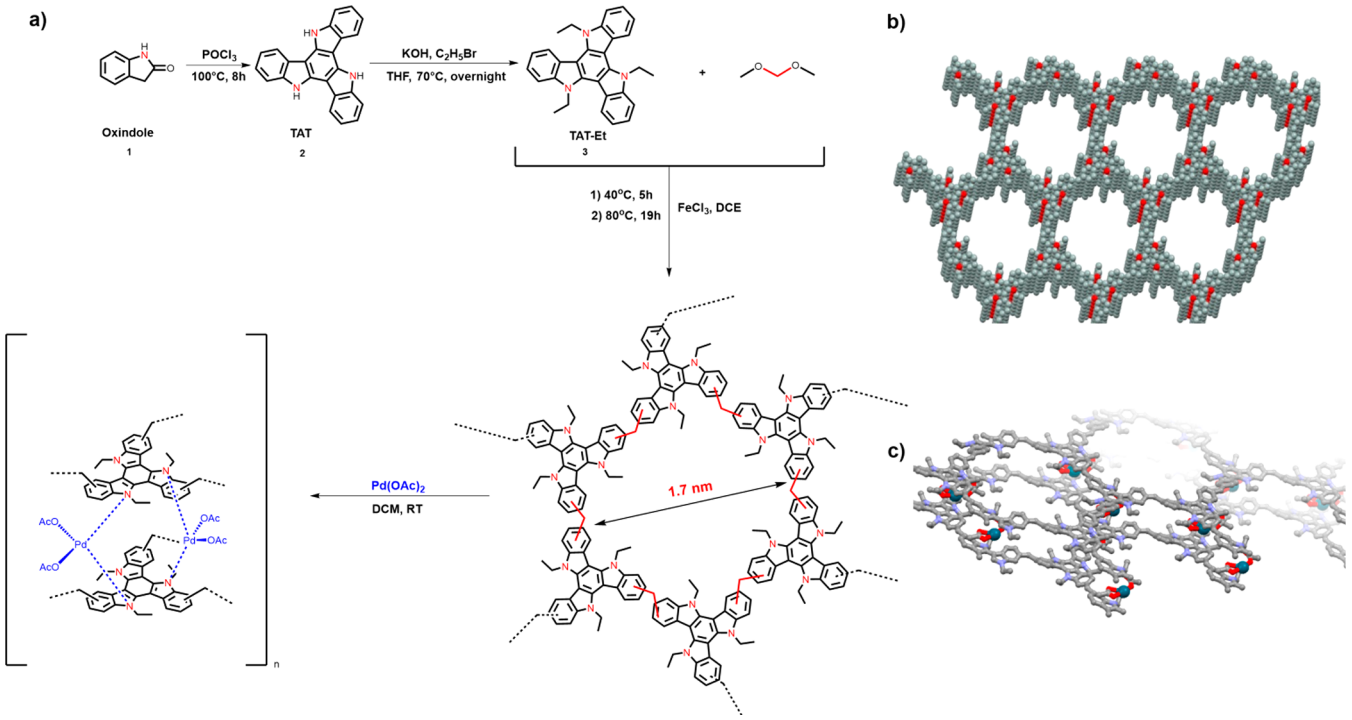

Figure 1. (a) Synthesis of TATHCP and TATHCP-Pd. (b, c) Proposed structures of TATHCP and TATHCP-Pd possessing regular microporous channels (diameter of ∼1.7 nm), simulated with a 3D eclipsed layered-sheet arrangement.

the yield of the TATHCP network synthesized by the knitting method was quantitative.[38,40] In the synthesis of triazatruxene (**2**) monomer, 2-oxoindole (**1**) was first refluxed in $POCl_3$. Because of the low solubility of the resulting trimer structure in organic solvents, N-alkylation of nitrogen groups with 1-bromododecane was performed. Due to the low surface area (24 m^2/g) of the product obtained from the first reaction, the area of HCP was increased to 997 m^2/g by changing the length of the alkyl chain, the equivalent amounts of the substances and reaction solvent. The N-alkylation of the short-chain ethyl group to the TAT nitrogens resulted in the largest skeletal structure of TATHCP, while the flexible and short chains were more successful in preventing clogging of the micropores when compared to the long chain alkyl groups. (Table S8, Supporting Information). Palladium(II) coordination reaction of HCP material was carried out by treatment of TATHCP with $Pd(OAc)_2$ at room temperature to obtain TATHCP-Pd material. Pd(II)-coordination of the synthesized TATHCP-Pd was confirmed by energy-dispersive X-ray spectroscopy (EDX), powder X-ray diffraction (PXRD), inductively coupled plasma (ICP), X-ray photoelectron spectroscopy (XPS) and solid-state NMR spectroscopy. One of the common and effective techniques used in the formation of C−C bonds is the Suzuki−Miyaura reaction, which is the cross-coupling reaction of aryl halides with aryl boronic acids.[41] However, using homogeneous Pd in that type reactions, recovery of complexes from the reaction mixture is difficult and Pd catalyst cannot be readily recycled for the next round of reaction. The use of Pd-supported MOF and COF was found to have an important effect on recyclability and the yields of products were not significantly reduced up to 5 cycles.[15,16] Similar to previously reported studies, when we investigated the catalytic activity of TATHCP-Pd material with a wide range of reagents in the Suzuki−Miyaura reaction, it was observed that TATHCP-Pd is a highly stable catalyst that can be easily recovered up to five cycles with excellent yields ranging from 97 to 98%. As shown in Figure 1, methylal crosslinked TATHCP material was synthesized in 1,2-dicholoroethane catalyzed by $FeCl_3$ under nitrogen environment (see Supporting Information for details). The ratios between TAT, methylal and $FeCl_3$ were 1:3:3. Due to the extensive hyper-cross-linking, the synthesized TATHCP network is insoluble in water as well as in many commonly used solvents such as dimethyl sulfoxide, trichloromethane, acetone, tetrahydrofuran, and *N*,*N*-dimethylformamide. Methanol, which can be readily separated from the material, is the only byproduct of the reaction. The spectral properties of polymeric network were investigated by FT-IR, SEM, TEM, XRD, and solid-state magic angle spinning (CP/MAS) ^{13}C NMR spectrometry, as shown in Figures S1−S5. FT-IR peaks show C═C (stretching) vibrations around 1080−1580 cm^{-1} while heteroatomic aromatic ring C−H vibrations (stretching) around 2970 cm^{-1} indicate that the polymer is highly cross-linked.

Stretching vibrations of the C−N−C moieties appear as characteristic bands at around 1450 cm^{-1} (Figure S1). EDX analysis was used to determine the purity of the resulting polymer. It was observed that $FeCl_3$, which was used as catalyst, was not present in the polymer obtained only by the determination of C and N elements (Figure S3, Supporting Information). The solid state ^{13}C CP-MAS NMR spectroscopy confirmed the atomic structure of TATHCP. Peak resonances at 129 and 142 ppm belong to fused rings, while the peak under 60 ppm belongs to the methylene carbon of the methylal. In addition, the peak resonance at about 107 ppm corresponds to the carbon atoms at the 3-position of the indole trimer, while the peak of the ethyl groups appears to be resonance at about 15 ppm. (Figure S5, Supporting Information). It was observed from the thermogravimetric analysis (TGA) spectrum (Figure S6, Supporting Information) that both polymeric networks TATHCP and TATHCP-Pd are

https://dx.doi.org/10.1021/acsaem.0c00539
ACS Appl. Energy Mater. 2020, 3, 4983−4994

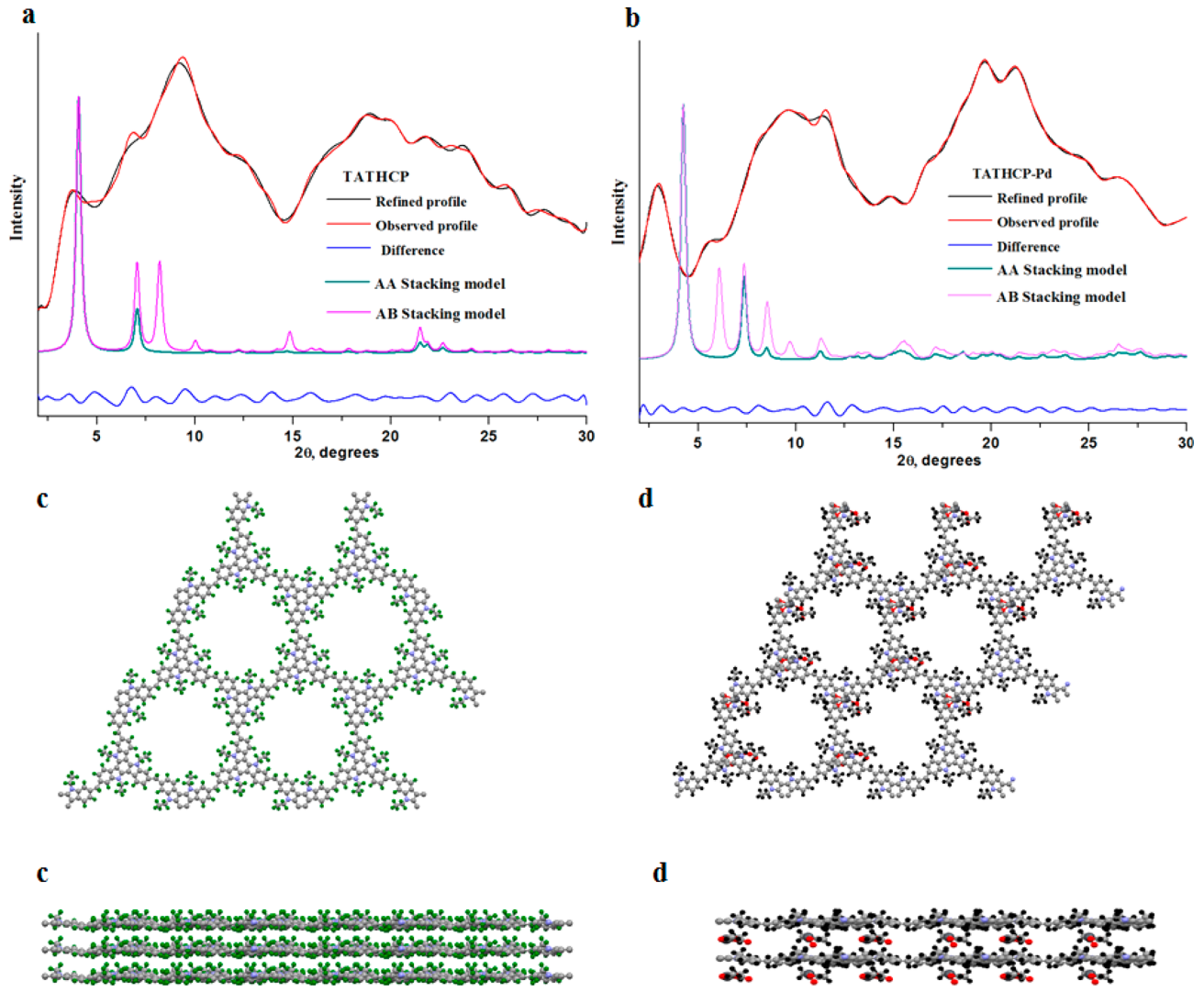

Figure 2. Observed (red) versus Pawley-refined (black) PXRD pattern profiles for eclipsed (a) TATHCP and (b) TATHCP-Pd structures. Residuals are indicated. View of the TATHCP (c) and TATHCP-Pd (d) structures on (001) planes and their layered structures. The refinement was done for amorphous compounds. The XRD profiles for AA and AB crystals stacking models are presented for comparison.

stable up to 400 °C, which meets potential application requirements in postcombustion CO_2 scrubbing operations and catalytic applications that occur at higher temperatures. However, TGA studies may not reveal the true stability of TATHCP-Pd because Pd sintering may take place without the thermal decomposition of the polymer. Both materials maintain more than 65% of their mass at temperatures over 800 °C which is most likely N-doped carbon as a result of thermal decomposition while the little weight loss (~4%) under 60 °C corresponds to trapped moisture and solvents in the pores.

Powder X-ray Analysis. The PXRD profiles of TATHCP and TATHCP-Pd compounds contain the low angle diffraction peaks in vicinities of 2θ values of 3.0−4.0° and 2.5−3.5°, respectively, which is characteristic for expected large unit-cell parameters. However, the presence of broad peaks on both profiles indicates amorphous−crystalline nature of the studied samples similarly like studied MOFs before.[42−44] Therefore, the geometry optimization of constructed models of TATHCP and TATHCP-Pd having the eclipsed topology was performed by an ABINIT code (see Supporting Information for details). The relaxed models were used for their powder X-ray diffraction patterns simulation in order to determine the structures of TATHCP and TATHCP-Pd. It was found that TATHCP compound has the fully eclipsed structure with an AA stacking sequence (Figure 2a) and the separation between the layers is equal to 4.135 Å. The structure of TATHCP-Pd, refined in the space group P1, contains two independent molecules of $Pd(OAc)_2$ in the asymmetric unit cell which are arranged between two TATHCP layers (Figure 2b) and confirmed by XPS analyses (Figure S17a,b). The distances of each of metals with the nitrogen atoms, located in the neighboring layers, are 3.082, 3.876 Å and 3.578, 3.817 Å, respectively and the separation between layers is 6.725 Å. The PXRD spectrum of TATHCP-Pd obtained from the coordination reaction with palladium acetate shows that the morphology of the structure is similar when compared with TATHCP. In addition, when ^{13}C CP/MAS NMR spectra are examined, the fact that the phenyl region of TATHCP-Pd is almost the same as that of TATHCP indicates that the structural preservation of TATHCP is maintained upon treatment with $Pd(OAc)_2$ (Figure S16).

The transmission electron microscopy (TEM) and scanning electron microscopy (SEM) images of the TATHCP-Pd show

https://dx.doi.org/10.1021/acsaem.0c00539
ACS Appl. Energy Mater. 2020, 3, 4983−4994

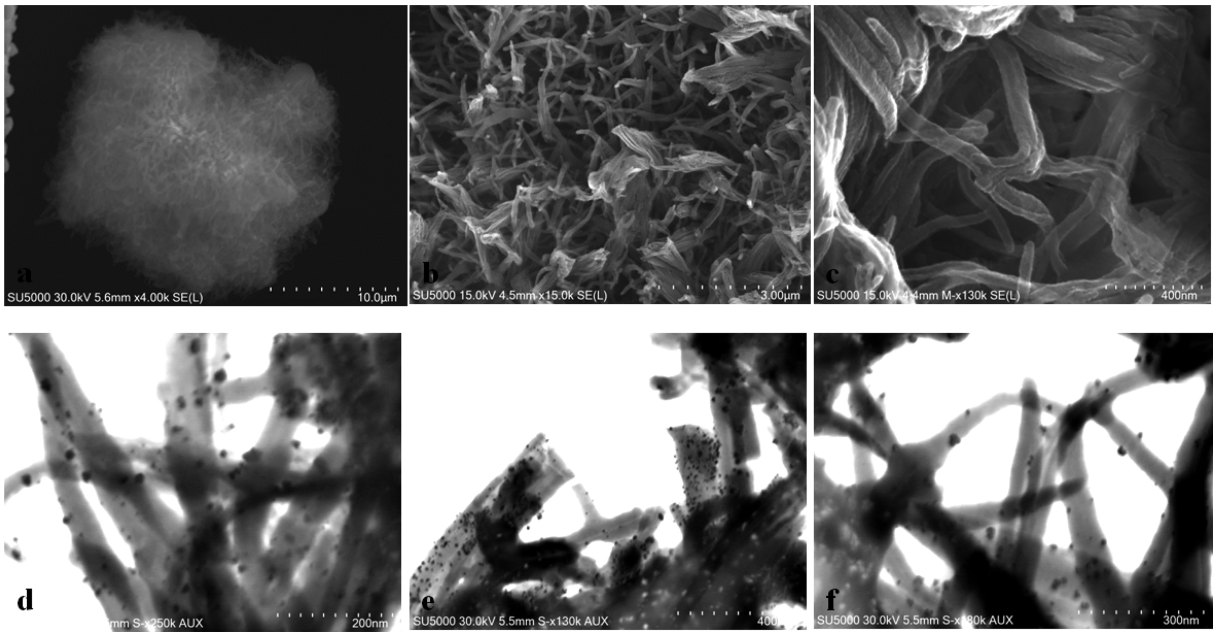

Figure 3. (a, b) SEM images of TATHCP and (c) TATHCP-Pd and (d, e) TEM images of TATHCP-Pd and (f) TATHCP-Pd-**Reuse**. See Supporting Information for more images.

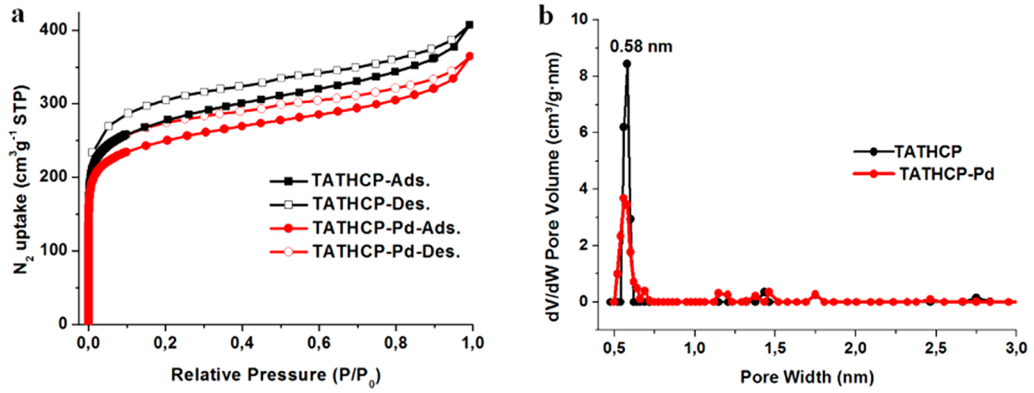

Figure 4. (a) N_2 adsorption−desorption isotherms and (b) pore size distribution of TATHCP and TATHCP-Pd.

that the Pd species (Figure 3, black dots[45] in parts d−f) are well dispersed on the support.[15] The Pd content in TATHCP-Pd is 4.2 ± 0.3 wt % as determined by ICP analysis. X-ray photoelectron spectroscopy (XPS) analysis was performed to see the binding energy of palladium which was estimated to be coordinated to the structure of TATHCP (Figure S17a). Black and green peaks are the binding energies (BE) of $Pd_{3d5/2}$ in TATHCP-Pd 335.3 and 337,8 eV indicating that the polymer contains two independent molecules of Pd fragments. The palladium atoms are present in +2 oxidation state in the asymmetric unit cell which is arranged between two TATHCP layers (Figure S17b).[46] Compared with $Pd(OAc)_2$, the free binding energy of 337.9 eV, TATHCP-Pd containing two independent $Pd(OAc)_2$ molecules with binding energies of 335.3 and 337.8 eV shifted negatively to 2.6 and 0.1 eV, respectively (Figure S17a, black). The tertiary nitrogens in TATHCP provide stronger coordination as they provide more electrons to the Pd (II) species, resulting in negative shifts compared to $Pd(OAc)_2$.

Porosity Studies. Nitrogen gas was used as a probe molecule at 77 K to determine the porosity and surface area of TATHCP and TATHCP-Pd (Figure 4). The sharply increasing adsorption in the low pressure range P/P_0 = 0−0.1 and the steady adsorption at higher pressures than 0.1 show that the obtained polymer structure has microporous character and a permanent micropore structure. The pore size distribution (PSD) was derived from nonlocal density functional theory (NLDFT) and found to be (0.58 nm). As depicted in (Figure 4b), the PSD curve indicates that the polymer has mostly (more than 60%) ultramicroporous character in nature. According to the IUPAC classification,[47] the TATHCP network, which is observed to be type I isotherm, has a predominantly centered ultra micropore pore structure at 0.58 nm, which is useful for gas storage and separation. However, the pore size predicted from molding studies is ∼1.7 nm. This discrepancy between the experimental and calculated pore size values is most likely due to the dominant amorphous nature of TATHCP and TATHCP-Pd. When Langmuir and Brunauer−Emmett−Teller (BET) models were used for surface area calculations, the values of TATHCP were calculated as 1215 $m^2\ g^{-1}$ and 997 $m^2\ g^{-1}$, respectively (Figure S7−S8). The degree of microporosity in the polymer material was calculated by taking the ratio of micropore volume to total pore volume ($V_{0.1}/V_t$), (Table 1).

https://dx.doi.org/10.1021/acsaem.0c00539
ACS Appl. Energy Mater. 2020, 3, 4983−4994

Table 1. Textural Properties of TATHCP and TATHCP-Pd

polymer	S_{BET} [a] [$m^2\ g^{-1}$]	S_{micro} [b] [$m^2\ g^{-1}$]	V_t [c] [$cm^3\ g^{-1}$]	$V_{0.1}$ [d] ($cm^3\ g^{-1}$)	% $V_{0.1}/V_t$	S_{micro}/S_{BET} [%]	$4V/A$ [e] $_{BET}$ [nm]
TATHCP	997	695	0.63	0.44	70	70	2.53
TATHCP-Pd	864	647	0.57	0.36	63	75	2.40

[a]Surface area calculated from N_2 adsorption isotherm in the relative pressure (P/P_0) range from 0.05 to 0.20. [b]Micropore surface area calculated from the N_2 adsorption isotherm using the *t*-plot method from the Harkins–Jura equation. [c]Total pore volume at P/P_0 = 0.99. [d]Micropore volume at P/P_0 = 0.1. [e]Average pore diameter.

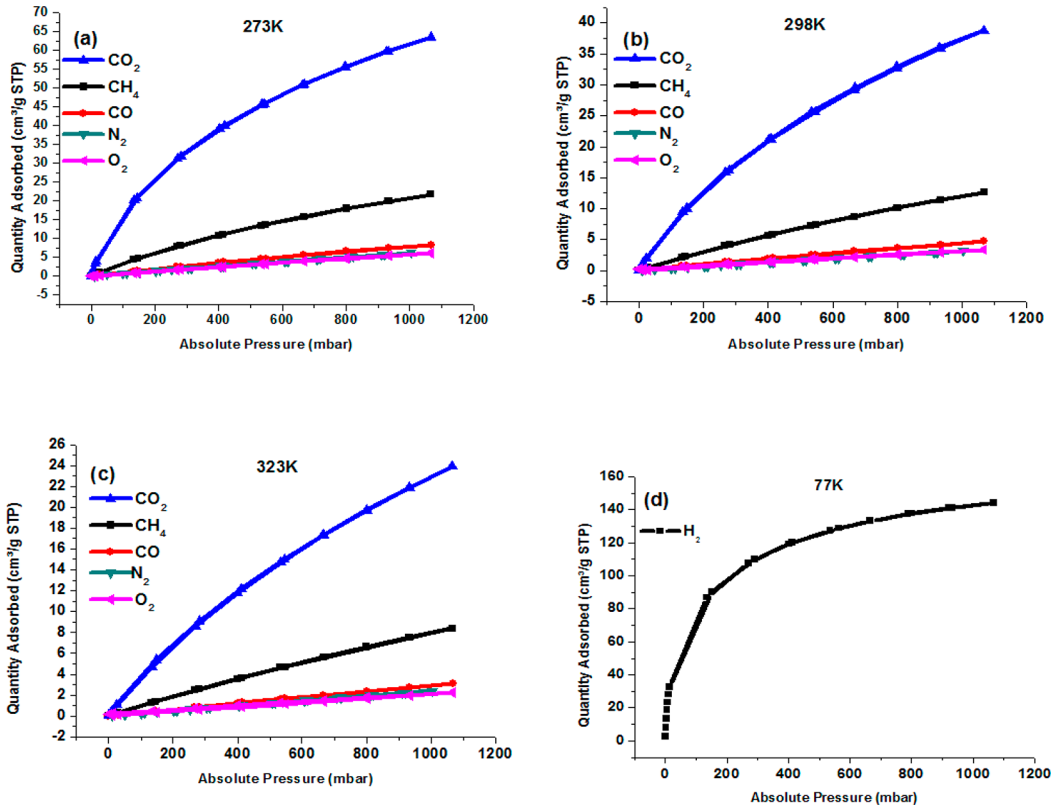

Figure 5. Gas adsorption/desorption isotherms of TATHCP at (a) 273 K, (b) 298 K, (c) 320 K, and (d) 77 K for H_2.

The micropore and total pore volume calculated at P/P_0 = 0.1 and 0.99 are 0.44 and 0.63 $cm^3\ g^{-1}$, respectively. The mild capillary condensation above P/P_0 0.90–0.95 of TATHCP, which is generally exhibited in microporous polymers, is caused by swelling of the polymer network during the contact of the interstitial voids with the adsorbate gas in the polymer.[24] Compared to TATHCP, the small change in pore size distribution and the moderate change in surface area of TATHCP-Pd indicate that Pd species do not cover the voids of the polymer, but only increase the weight of the building units. The micropore and total pore volume of TATHCP-Pd calculated at P/P_0 = 0.1 and 0.99 are 0.36 and 0.57 $cm^3\ g^{-1}$. It was observed from the thermogravimetric analysis (TGA) spectrum (Figure S6) that TATHCP-Pd is stable up to 450 °C, meeting potential application requirements in catalysis that usually occur at elevated temperatures. The interest in the use of recycled palladium catalysts in industrial applications remains attractive due to the difficulties encountered in the recycling and separation of expensive palladium catalysts.[48−50]

Gas Selectivity. High surface area and the ultramicroporous nature with an electron-rich conjugated system of TATHCP prompted us to study first its gas sorption properties. As shown in Figure 5 the CO_2, N_2, CH_4, CO, and O_2 adsorption isotherms were obtained at 273, 298, and 320 K from 0 to 1.1 bar. TATHCP's CO_2 uptake capacity is 12.55% by weight, 7.68% by weight, and 4.75% by weight at 273 K/1.1 bar, 298 K/1.1 bar, and 320 K/1.1 bar, respectively (Figure 6). The desorption isotherms are very close to adsorption profiles and therefore the CO_2 physisorption process is reversible. Impressively, these uptake values obtained for CO_2 at 273 K are not only higher than many materials with similar specific surface areas in the literature, but also close to many materials with larger specific surface areas,[51−53] BPL carbon, MOFs[54,55] (Table S1, S3) while lower or comparable than BILPs and ALPs.[53,54] Also, the CO_2 uptake capacity of TATHCP at 298 K is significantly higher than many reported HCP materials[24] (Table S3) while lower or comparable than BILPs and ALPs.[53,54] This high affinity of the polymer to CO_2 is due to a high amount of nitrogen atoms which have unpaired electrons on the polymer cause increased adsorption properties.[56] Using the Clausius–Clapeyron equation, the isosteric heat of adsorption (Q_{st}) of TATHCP at zero loading was calculated as 32.66 kJ/mol^{-1} for CO_2 uptake (Figure S11). Despite the increased amount of adsorption, the heats of adsorption remain at 28 kJ mol^{-1}, indicating that the polymer has a good CO_2 retention capacity despite its moderately low surface area. The Q_{st} value not exceeding 50 kJ mol^{-1} indicates that the polymer structure physically adsorbs CO_2, while weak

https://dx.doi.org/10.1021/acsaem.0c00539
ACS Appl. Energy Mater. 2020, 3, 4983−4994

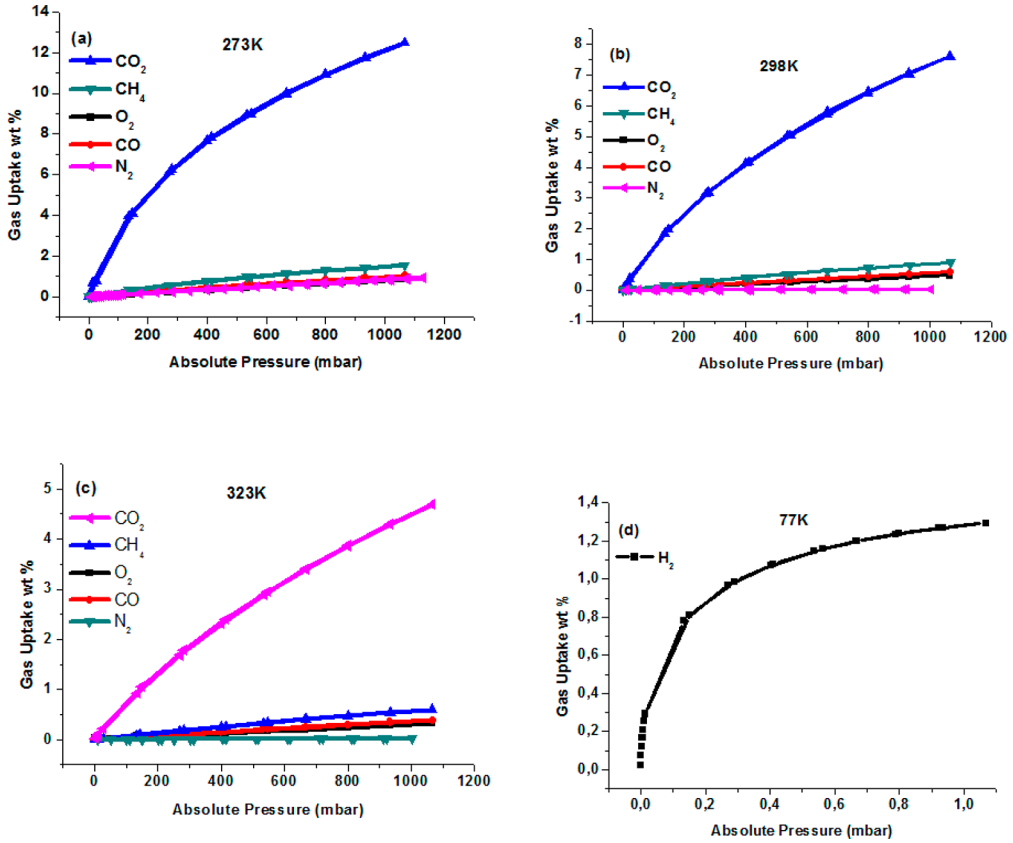

Figure 6. Gas adsorption selectivities (% wt) of TATHCP at (a) 273, (b) 298, (c) 320, and (d) 77 K for H_2.

interactions between CO_2 and the polymer provide recyclability of the adsorbent without consuming much energy. Gas uptake studies for CH_4 and H_2, obtain the needed storage levels there must be used much higher pressure, however, low pressure (1 bar) uptakes can be check for subsequent gas separation studies at ambient pressure. Physical adsorption of methane can be a more economical and safer compared to storage at low pressures and in compressed form.[57]

Adsorption properties of TATHCP network were therefore investigated at 273, 298, and 320 K using methane as probe gas. The CH_4 uptakes of TATHCP at 1.1 bar are 1.56, 0.90, and 0.60 wt % at 273, 298, and 320 K, respectively (Figure 6). The obtained values are comparable or higher than the recently reported networks[14,58−63](Table S4). The Q_{st} of CH_4 was calculated by using adsorption data obtained at 273 and 298 K (Figure S12), which shows that TATHCP exhibits 20.65 kJ mol^{-1} at zero coverage. The smaller Q_{st} value of CH_4 compared to that of CO_2 are due to its nonpolar nature. In addition, the physical absorption of hydrogen from porous materials is an extremely important issue in clean energy applications. As a result of H_2 sorption isotherm measurement at 77 K (Figure 5) and 1.1 bar, it was observed that TATHCP has 1.30 wt % H_2 uptake capacity (Figure 6). The observed uptake value is considerable when compared with previous studies and it is seen that saturation is not reached from the adsorption curve, and higher H_2 capacity can be obtained under higher pressures[5,60,64] (Table S5).

To determine of TATHCP's CO_2 separation abilities over O_2 and CO, adsorption properties of the network were further characterized probed by using O_2 and COat 273, 298, and 320 K at 1.1 bar. The O_2 uptake of TATHCP at 1.1 bar is 0.88, 0.48, and 0.31 wt % at 273, 298, and 320 K while the CO uptake of TATHCP at 1.1 bar is 1.04 wt % at 273 K, 0.58 wt % at 298 K, and 0.38 wt % at 320 K, respectively (Figure 6).

A polymer material must have high CO_2 uptake capacity and reversibility as well as high CO_2/N_2 selectivity, which is essential for use as a CO_2 adsorbent. Myers and Prausnitz's ideal adsorbed solution theory (IAST) is one of the methods used to predict multicomponent adsorption behavior from experimental single-component gas isotherms.[65] The selectivity values of TATHCP material for five different gases (CO_2, CH_4, N_2, CO, and O_2) under three different temperature (273, 298, and 320 K) conditions were calculated up to 1 bar using IAST. The TATHCP's CO_2/N_2 (15/85) selectivities calculated at 1.1 bar were 38.4 at 273 K, 22.3 at 298 K, and 15.7 at 320 K, close to 37.5 at 273 K, 24.1 at 298 K and 15.6 at 320 K better than most lately reported materials (Tables S2 and S6, and Figures S13−S15).[33,66−69]

In the purification of natural gas, CO_2 must be separated from CH_4.[24] As a result of this purification, both the energy efficiency is increased and the corrosion of the pipeline is prevented. The calculated CO_2/CH_4 (50/50) selectivity at 1.1 bar of TATHCP is 7.8 at 273 K, 5.2 at 298 K, and 4.16 at 320 K while 7.9 at 273 K, 4.8 at 298 K, and 4.1 at 320 K for (5/95), respectively. The selectivity at 273 K is higher than those of reported porous networks (Table S7).[66,70,71] In addition, the selectivity values of CO_2 over O_2 and CO were calculated at 273, 298, and 323 K (Figures S13−S15). Selectivity values of CO_2/O_2 are 40.6, 25.5, and 18.0 while those for CO_2/CO are 32.1, 18.6, and 13.2 at 273, 298, and 323 K respectively. From these results, TATHCP emerges as a good candidate for CO_2 separation in flue gas separation processes (CO_2−N_2, CO_2−O_2, CO_2−CO, CO_2−CH_4).

https://dx.doi.org/10.1021/acsaem.0c00539
ACS Appl. Energy Mater. 2020, 3, 4983−4994

Catalytic Activity. The catalytic activity of the TATHCP-Pd and its reversibility were investigated in the Suzuki–Miyaura coupling reaction, one of the most well-known Pd catalyzed reactions. In order to compare the reaction results and yields, the catalytic reactions were performed using the same reactants and similar conditions in COF and MOF materials previously reported.[72] The results are summarized in Table 2. Product yields of aryl boronic acids with aryl bromides in the reactions catalyzed by 0.5% TATHCP-Pd are excellent, ranging from 90 to 98%. Although less active than the iodide group, the reaction yields of all aryl bromides except 4-bromoanisole (90%) were excellent, and the reactions were completed within 3.5 to 4 h at 150 °C. When half the amount, 0.25 mol % of catalyst was used, the reaction was still complete although with prolonged reaction time (10 h) (entry 9) (Tables 2 and 3).

Table 2. Catalytic Activity Test of TATHCP-Pd in the Suzuki–Miyaura Coupling Reaction

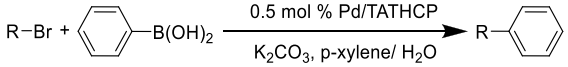

Entry[a]	R	Time (h)	Yield[b] (%)	TON[d]
1	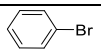	3.5	95	190
2	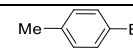	3.5	96	192
3	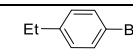	3.5	96	192
4	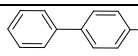	4.0	94	188
5	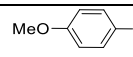	4.0	90	180
6	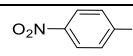	3.5	98	196
7	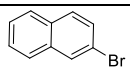	4.0	92	184
8	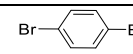	4.0	94	188
9[c]	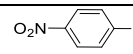	10.0	96	192

[a]Unless otherwise indicated, the reaction conditions are: aryl bromide (1 mmol), phenylboronic acid (0.75 mmol), K_2CO_3 (0.5 mmol), 4 mL of p-xylene, 0.2 mL of H_2O, 150 °C. [b]NMR yields. [c]0.25 mol % TATHCP-Pd was used. [d]TON, turnover number [(mol of product)/(mol of catalyst)].

Considering all these results, it is seen that TATHCP-Pd has high catalytic activity in Suzuki–Miyaura cross coupling reactions. In comparison with the Pd(II)-containing MOF,[73] TATHCP-Pd required the same catalyst-loading with MOF and nearly the same reaction times with Pd/COF-LZU1,[15] which shows almost the same reaction yields and turnover numbers.

Table 3. Recycle Test of TATHCP-Pd in the Suzuki–Miyaura Cross-Coupling Reaction of *p*-NBB and PBA

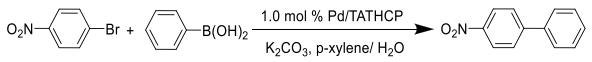

entry	time (h)	% yield[a]	TON[b]
fresh	3.5	98	98
cycle 1	3.5	96	96
cycle 2	3.5	95	95
cycle 3	3.5	96	96
cycle 4	3.5	94	94

[a]NMR yields. [b]TON, turnover number [(mol of product)/(mol of catalyst)].

Since TATHCP-Pd is a robust, inexpensive structure, it would be more appealing for industrial applications. Given the possibility of $Pd(OAc)_2$ leaking from TATHCP-Pd, three different paths were followed to determine whether the reactions were catalyzed with free $Pd(OAc)_2$ leaking from the polymer material or with $Pd(OAc)_2$ coordinated with TATHCP-Pd. First, reaction media containing TATHCP-Pd, *p*-xylene, and potassium carbonate except for reactants and was heated and stirred at 150 °C for 10 h. The ICP analysis results indicate that the palladium content was found 0.0018%wt. Then as a blank reaction was established again without TATHCP-Pd and ICP results showed that amount of palladium was determined as 0.0017 wt %. These results demonstrate that there was no Pd leaked out into the reaction media. Finally, TATHCP-Pd was removed after 50% conversion of the reagents and no increase in product yield was observed when the remaining mixture was maintained under the same reaction conditions (Figure S18). We believe that the high degree of gas adsorptive properties of TATHCP as well as the superior activity of the TATHCP-Pd catalyst could be ascribed to the planar construction of TAT and due to the formation of each channel (2.53 nm) in the network cross-linked by methylal. Furthermore, the distance of the tertiary nitrogen atoms between ordered layers is 4.16 Å, which meets the ideal requirements for the Pd moieties to have strong coordination with the material. The reuse of the TATHCP-Pd in Suzuki–Miyaura coupling can be explained that the catalyst has excess nitrogen functionalities in the network coordinating and thus stabilizing the $Pd(OAc)_2$ species. The porous properties of the TATHCP can provide steric limitation for the $Pd(OAc)_2$ species and thus to prevent the formation of metal clusters.

Thermoelectric Transport Coefficients and Band Structures. Recently, the two-dimensional fluorene-based covalent organic framework (FL-COF) doped by iodine displayed a high Seebeck coefficient with a well thermoelectric performance at room temperature in spite that I2@FL-COF was obtained as amorphous framework.[74] Moreover, it was shown that phthalocyanine (Pc) based NiPc COF exhibits both high Seebeck coefficients on sides *a*- and *b*- and figures of merit *ZT*, making it an extra-performance n-type thermoelectric network in the *in plane* direction.[75] Because we observed layered structure in TATHCP, the Boltzmann transport equation and the density functional theory were, therefore, applied for the structures of TATHCP and TATHCP-Pd to estimate their semiclassical transport coefficients (see Supporting Information for details).

The band structures of TATHCP and TATHCP-Pd are presented in Figure 7. According to the results obtained, the

https://dx.doi.org/10.1021/acsaem.0c00539
ACS Appl. Energy Mater. 2020, 3, 4983–4994

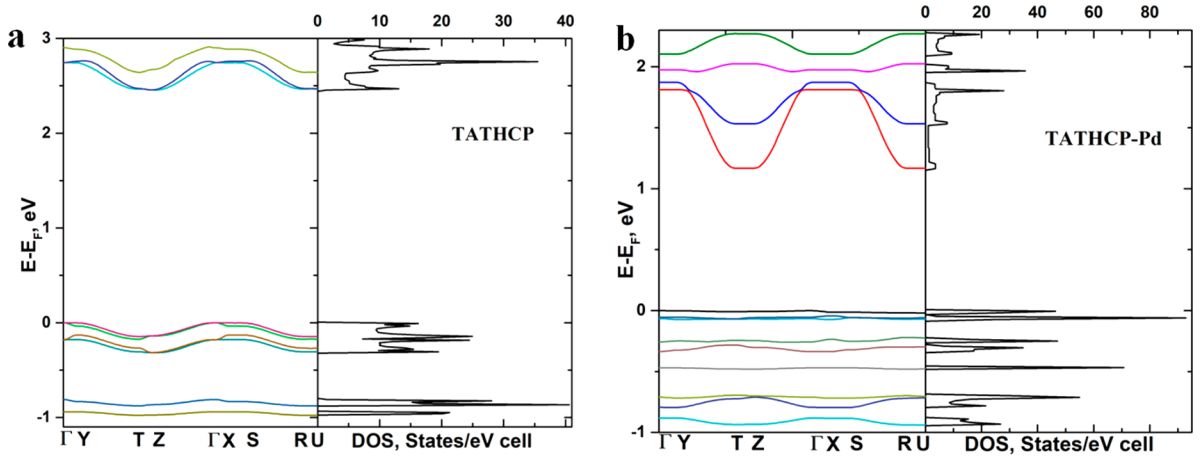

Figure 7. Band structures and DOS of TATHCP and TATHCP-Pd. The reciprocal coordinates of high-symmetry points are Γ = (0, 0, 0), *X* = (0.5, 0, 0), *Y* = (0, 0.5, 0), *Z* = (0, 0, 0.5), *S* = (0.5, 0.5, 0), *U* = (0.5, 0, 0.5), *T* = (0, 0.5, 0.5), and *R* = (0.5, 0.5, 0.5).

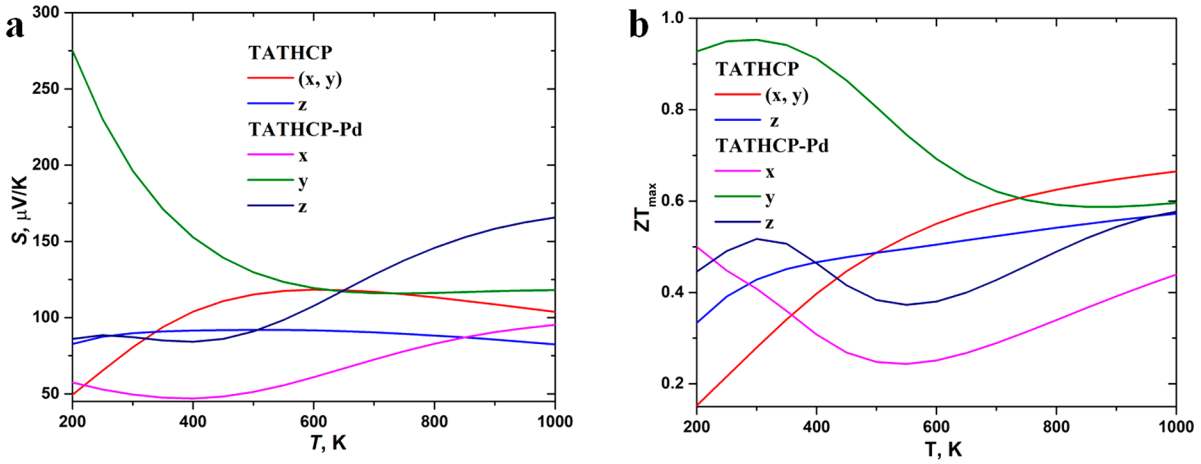

Figure 8. Theoretical anisotropic temperature dependence of (a) thermopower and (b) dimensionless figure of merit *ZT* calculated by BoltzTraP for TATHCP and TATHCP-Pd along the three axes.

TATHCP-Pd has a direct bandgap of 1.17 eV. In addition, both the conduction band (CB) minimum and the valence band (VB) maximum are located very close to the *Z* point. The band structure of TATHCP, where CB minima VB maxima is located at *Z* and Γ points, shows that this structure has semiconductor properties and has an energy gap of 2.45 eV at the ground state.

The conduction band in both materials exhibits quite complex behavior because the bands exhibit crossovers, minima and maxima. Along all high-symmetry lines near the Fermi energy level there are some practically flat subband dispersions in the valence-band of TATHCP-Pd that are related to narrow sharp peaks of the density of states (DOS). This means that the masses acting in the respective directions in the k-space are very massive, indicating that the carriers are localized in the potential walls. Unlike in TATHCP-Pd, the VB of TATHCP displays quite complicated behavior near Fermi energy level because the bands exhibit crossovers, minima and maxima practically along all high-symmetry lines that led to peaks broadening of DOS. The calculated anisotropic temperature dependency of Seebeck coefficients and figures of merit, based on band structures of TATHCP and TATHCP-Pd are presented in Figure 8. Electron scattering time is obtained by the term of the Seebeck coefficient due to the continuous relaxation time predicted in the BoltzTraP approach. For this reason, this value can be calculated as an absolute figure and give a better control to compare with the measured values. Considering these important positive thermopower values found for TATHCP and TATHCP-Pd, it can be said that hole-type carrier is dominant in thermoelectric transport for these materials. The maximal values of both Seebeck coefficients and ZT_{max} are observed along the *y*-direction in the temperature interval of 200−600 K for TATHCP-Pd and their meanings range from 276 to 119 μV/K and from 0.95 to 0.64 respectively. The existence of localized states in VB of this compound may prevent the electron−hole compensation effect that correlates with the large values of thermopowers and ZT_{max}. For TATHCP the maximal values of *S* and ZT_{max} are observed along *x*- and *y*-axes (*in plane* direction) in temperature interval of 500−1000 K, and their values range from 103 to 118 μV/K and from 0.49 to 0.66, respectively.

CONCLUSION

In summary, a new hyper-cross-linked microporous organic polymer network TATHCP from a planar trimer indole building block has been synthesized via Friedel−Crafts alkylation using a methylal linker and anhydrous $FeCl_3$. The properties of the synthesized polymer structure were

https://dx.doi.org/10.1021/acsaem.0c00539
ACS Appl. Energy Mater. 2020, 3, 4983−4994

investigated in gas adsorptions, metal coordinated catalytic applications and thermoelectric activities. The high gas adsorptive properties of TATHCP provide great potential for extraction of CO_2 in flue gas separation processes, coupled with the superior catalytic activity of TATHCP-Pd; also, their robust and inexpensive structures make them highly attractive for industrial applications. The thermoelectric properties of TATHCP materials are surprisingly promising, and with the optimization of the 2D stacking of network polymer layers, effective devices could be fabricated. Our efforts will continue on exploring this potential.

■ ASSOCIATED CONTENT

Supporting Information

The Supporting Information is available free of charge at https://pubs.acs.org/doi/10.1021/acsaem.0c00539.

Experimental part (materials and methods, synthesis), FT-IR spectra, PXRD patterns, Pawley refinement modeling details, gas adsorption, isosteric heat of adsorption for CO_2 and CH_4, TGA data, SEM images, TEM images, EDS images and spectra, solid-state ^{13}C CP-MAS NMR spectra, theoretical calculations, and adsorption selectivities of CO_2 over N_2, CH_4, O_2, and CO and tables of selectivity, gas adsorption capacity, and CO_2, CH_4, and H_2 uptake comparison of different microporous materials (PDF)

■ AUTHOR INFORMATION

Corresponding Authors

Ali Enis Sadak − *Chemistry Group Laboratories, TUBITAK UME, 41470 Gebze, Kocaeli, Turkey;* orcid.org/0000-0002-5065-8236; Email: alienis.sadak@tubitak.gov.tr

Erman Karakuş − *Chemistry Group Laboratories, TUBITAK UME, 41470 Gebze, Kocaeli, Turkey;* orcid.org/0000-0002-2691-8704; Email: erman.karakus@tubitak.gov.tr

Authors

Yurii M. Chumakov − *Department of Physics, Gebze Technical University, 41400 Gebze, Kocaeli, Turkey*

Nesibe A. Dogan − *Department of Chemical and Biomolecular Engineering, Korea Advanced Institute of Science and Technology (KAIST), Daejeon 34141, Republic of Korea*

Cafer T. Yavuz − *Department of Chemical and Biomolecular Engineering, Korea Advanced Institute of Science and Technology (KAIST), Daejeon 34141, Republic of Korea;* orcid.org/0000-0003-0580-3331

Complete contact information is available at: https://pubs.acs.org/10.1021/acsaem.0c00539

Author Contributions

‡A.E.S. and E.K. contributed equally

Notes

The authors declare no competing financial interest.

■ ACKNOWLEDGMENTS

The authors gratefully acknowledge TUBİTAK-UME for financial support and thank Muhiddin CERGEL and Ilker UN for NMR analysis, Murat TUNC for ICP analysis and Gokhan BILSEL for HRMS analysis. N.A.D. and C.T.Y. acknowledge funding support from the National Research Foundation of Korea (NRF-2017M3A7B4042140).

■ REFERENCES

(1) McKeown, N. B.; Budd, P. M. Polymers of intrinsic microporosity (PIMs): organic materials for membrane separations, heterogeneous catalysis and hydrogen storage. *Chem. Soc. Rev.* **2006**, *35* (8), 675−683.

(2) Li, B.; Su, F.; Luo, H.-K.; Liang, L.; Tan, B. Hypercrosslinked microporous polymer networks for effective removal of toxic metal ions from water. *Microporous Mesoporous Mater.* **2011**, *138* (1), 207−214.

(3) Du, X.; Sun, Y.; Tan, B.; Teng, Q.; Yao, X.; Su, C.; Wang, W. Tröger's base-functionalised organic nanoporous polymer for heterogeneous catalysis. *Chem. Commun.* **2010**, *46* (6), 970−972.

(4) Dang, D.; Wu, P.; He, C.; Xie, Z.; Duan, C. Homochiral Metal-Organic Frameworks for Heterogeneous Asymmetric Catalysis. *J. Am. Chem. Soc.* **2010**, *132* (41), 14321−14323.

(5) Furukawa, H.; Yaghi, O. M. Storage of Hydrogen, Methane, and Carbon Dioxide in Highly Porous Covalent Organic Frameworks for Clean Energy Applications. *J. Am. Chem. Soc.* **2009**, *131* (25), 8875−8883.

(6) McKeown, N. B.; Gahnem, B.; Msayib, K. J.; Budd, P. M.; Tattershall, C. E.; Mahmood, K.; Tan, S.; Book, D.; Langmi, H. W.; Walton, A. Towards Polymer-Based Hydrogen Storage Materials: Engineering Ultramicroporous Cavities within Polymers of Intrinsic Microporosity. *Angew. Chem.* **2006**, *118* (11), 1836−1839.

(7) Wood, C. D.; Tan, B.; Trewin, A.; Su, F.; Rosseinsky, M. J.; Bradshaw, D.; Sun, Y.; Zhou, L.; Cooper, A. I. Microporous Organic Polymers for Methane Storage. *Adv. Mater.* **2008**, *20* (10), 1916−1921.

(8) Li, B.; Huang, X.; Liang, L.; Tan, B. Synthesis of uniform microporous polymer nanoparticles and their applications for hydrogen storage. *J. Mater. Chem.* **2010**, *20* (35), 7444−7450.

(9) Holst, J. R.; Cooper, A. I. Ultrahigh Surface Area in Porous Solids. *Adv. Mater.* **2010**, *22* (45), 5212−5216.

(10) Côté, A. P.; Benin, A. I.; Ockwig, N. W.; O'Keeffe, M.; Matzger, A. J.; Yaghi, O. M. Porous, Crystalline, Covalent Organic Frameworks. *Science* **2005**, *310* (5751), 1166−1170.

(11) El-Kaderi, H. M.; Hunt, J. R.; Mendoza-Cortés, J. L.; Côté, A. P.; Taylor, R. E.; O'Keeffe, M.; Yaghi, O. M. Designed Synthesis of 3D Covalent Organic Frameworks. *Science* **2007**, *316* (5822), 268−272.

(12) Férey, G.; Mellot-Draznieks, C.; Serre, C.; Millange, F.; Dutour, J.; Surblé, S.; Margiolaki, I. A Chromium Terephthalate-Based Solid with Unusually Large Pore Volumes and Surface Area. *Science* **2005**, *309* (5743), 2040−2042.

(13) Jiang, J.-X.; Cooper, A. I. Microporous Organic Polymers: Design, Synthesis, and Function. *Top. Curr. Chem.* **2009**, *293*, 1.

(14) Tozawa, T.; Jones, J. T. A.; Swamy, S. I.; Jiang, S.; Adams, D. J.; Shakespeare, S.; Clowes, R.; Bradshaw, D.; Hasell, T.; Chong, S. Y.; Tang, C.; Thompson, S.; Parker, J.; Trewin, A.; Bacsa, J.; Slawin, A. M. Z.; Steiner, A.; Cooper, A. I. Porous organic cages. *Nat. Mater.* **2009**, *8*, 973.

(15) Ding, S.-Y.; Gao, J.; Wang, Q.; Zhang, Y.; Song, W.-G.; Su, C.-Y.; Wang, W. Construction of Covalent Organic Framework for Catalysis: Pd/COF-LZU1 in Suzuki−Miyaura Coupling Reaction. *J. Am. Chem. Soc.* **2011**, *133* (49), 19816−19822.

(16) Corma, A.; García, H.; Llabrés i Xamena, F. X. Engineering Metal Organic Frameworks for Heterogeneous Catalysis. *Chem. Rev.* **2010**, *110* (8), 4606−4655.

(17) Davankov, V. A.; Tsyurupa, M. P. Structure and properties of hypercrosslinked polystyrene—the first representative of a new class of polymer networks. *React. Polym.* **1990**, *13* (1), 27−42.

(18) Rozyyev, V.; Thirion, D.; Ullah, R.; Lee, J.; Jung, M.; Oh, H.; Atilhan, M.; Yavuz, C. T. High-capacity methane storage in flexible alkane-linked porous aromatic network polymers. *Nature Energy* **2019**, *4* (7), 604−611.

(19) Tsyurupa, M. P.; Davankov, V. A. Porous structure of hypercrosslinked polystyrene: State-of-the-art mini-review. *React. Funct. Polym.* **2006**, *66* (7), 768−779.

(20) Belyakova, L. D.; Schevchenko, T. I.; Davankov, V. A.; Tsyurupa, M. P. Sorption of vapors of various substances by hypercrosslinked "styrosorb" polystyrenes. *Adv. Colloid Interface Sci.* **1986**, *25*, 249−266.
(21) Davankov, V. A.; Pastukhov, A. V.; Tsyurupa, M. P. Unusual mobility of hypercrosslinked polystyrene networks: Swelling and dilatometric studies. *J. Polym. Sci., Part B: Polym. Phys.* **2000**, *38* (11), 1553−1563.
(22) Molla, R. A.; Bhanja, P.; Ghosh, K.; Islam, S. S.; Bhaumik, A.; Islam, S. M. Pd Nanoparticles Decorated on Hypercrosslinked Microporous Polymer: A Highly Efficient Catalyst for the Formylation of Amines through Carbon Dioxide Fixation. *ChemCatChem* **2017**, *9* (11), 1939−1946.
(23) Bhunia, S.; Banerjee, B.; Bhaumik, A. A new hypercrosslinked supermicroporous polymer, with scope for sulfonation, and its catalytic potential for the efficient synthesis of biodiesel at room temperature. *Chem. Commun.* **2015**, *51* (24), 5020−5023.
(24) Saleh, M.; Lee, H. M.; Kemp, K. C.; Kim, K. S. Highly Stable CO_2/N_2 and CO_2/CH_4 Selectivity in Hyper-Cross-Linked Heterocyclic Porous Polymers. *ACS Appl. Mater. Interfaces* **2014**, *6* (10), 7325−7333.
(25) Fang, D.; Li, X.; Zou, M.; Guo, X.; Zhang, A. Carbazole-functionalized hyper-cross-linked polymers for CO2 uptake based on Friedel−Crafts polymerization on 9-phenylcarbazole. *Beilstein J. Org. Chem.* **2019**, *15*, 2856−2863.
(26) Xiong, S.; Tang, X.; Pan, C.; Li, L.; Tang, J.; Yu, G. Carbazole-Bearing Porous Organic Polymers with a Mulberry-Like Morphology for Efficient Iodine Capture. *ACS Appl. Mater. Interfaces* **2019**, *11* (30), 27335−27342.
(27) Zhu, X.; Mahurin, S. M.; An, S.-H.; Do-Thanh, C.-L.; Tian, C.; Li, Y.; Gill, L. W.; Hagaman, E. W.; Bian, Z.; Zhou, J.-H.; Hu, J.; Liu, H.; Dai, S. Efficient CO2 capture by a task-specific porous organic polymer bifunctionalized with carbazole and triazine groups. *Chem. Commun.* **2014**, *50* (59), 7933−7936.
(28) Ji, L.; Fang, Q.; Yuan, M.-s.; Liu, Z.-q.; Shen, Y.-x.; Chen, H.-f. Switching High Two-Photon Efficiency: From 3,8,13-Substituted Triindole Derivatives to Their 2,7,12-Isomers. *Org. Lett.* **2010**, *12* (22), 5192−5195.
(29) Bura, T.; Leclerc, N.; Bechara, R.; Lévêque, P.; Heiser, T.; Ziessel, R. Triazatruxene-Diketopyrrolopyrrole Dumbbell-Shaped Molecules as Photoactive Electron Donor for High-Efficiency Solution Processed Organic Solar Cells. *Adv. Energy Mater.* **2013**, *3* (9), 1118−1124.
(30) Ruiz, C.; López Navarrete, J. T.; Ruiz Delgado, M. C.; Gómez-Lor, B. Triindole-Bridge-Triindole Dimers as Models for Two Dimensional Microporous Polymers. *Org. Lett.* **2015**, *17* (9), 2258−2261.
(31) Shao, J.; Guan, Z.; Yan, Y.; Jiao, C.; Xu, Q.-H.; Chi, C. Synthesis and Characterizations of Star-Shaped Octupolar Triazatruxenes-Based Two-Photon Absorption Chromophores. *J. Org. Chem.* **2011**, *76* (3), 780−790.
(32) Lai, W.-Y.; He, Q.-Y.; Zhu, R.; Chen, Q.-Q.; Huang, W. Kinked Star-Shaped Fluorene/ Triazatruxene Co-oligomer Hybrids with Enhanced Functional Properties for High-Performance, Solution-Processed, Blue Organic Light-Emitting Diodes. *Adv. Funct. Mater.* **2008**, *18* (2), 265−276.
(33) Xie, Y.-F.; Ding, S.-Y.; Liu, J.-M.; Wang, W.; Zheng, Q.-Y. Triazatruxene based covalent organic framework and its quick-response fluorescence-on nature towards electron rich arenes. *J. Mater. Chem. C* **2015**, *3* (39), 10066−10069.
(34) Li, X.-C.; Zhang, Y.; Wang, C.-Y.; Wan, Y.; Lai, W.-Y.; Pang, H.; Huang, W. Redox-active triazatruxene-based conjugated microporous polymers for high-performance supercapacitors. *Chem. Sci.* **2017**, *8* (4), 2959−2965.
(35) Yang, X.; Yu, M.; Zhao, Y.; Zhang, C.; Wang, X.; Jiang, J.-X. Hypercrosslinked microporous polymers based on carbazole for gas storage and separation. *RSC Adv.* **2014**, *4* (105), 61051−61055.
(36) Singh, G.; Singh, P. A.; Sen, A. K.; Singha, K.; Dubeya, S. N.; Handa, R. N.; Choi, J. Synthesis and Characterization of Some Bivalent Metal Complexes of Schiff Bases Derived From as-Triazine. *Synth. React. Inorg. Met.-Org. Chem.* **2002**, *32* (1), 171−187.
(37) Sadak, A. E.; Gören, A. C.; Bozdemir, Ö. A.; Saraçoğlu, N. Synthesis of Novel meso-Indole- and meso-Triazatruxene-BODIPY Dyes. *ChemistrySelect* **2017**, *2* (32), 10512−10516.
(38) Li, B.; Gong, R.; Wang, W.; Huang, X.; Zhang, W.; Li, H.; Hu, C.; Tan, B. A New Strategy to Microporous Polymers: Knitting Rigid Aromatic Building Blocks by External Cross-Linker. *Macromolecules* **2011**, *44* (8), 2410−2414.
(39) Xu, S.; Luo, Y.; Tan, B. Recent Development of Hypercrosslinked Microporous Organic Polymers. *Macromol. Rapid Commun.* **2013**, *34* (6), 471−484.
(40) Shen, R.; Yan, X.; Guan, Y.-J.; Zhu, W.; Li, T.; Liu, X.-G.; Li, Y.; Gu, Z.-G. One-pot synthesis of a highly porous anionic hypercrosslinked polymer for ultrafast adsorption of organic pollutants. *Polym. Chem.* **2018**, *9* (38), 4724−4732.
(41) Miyaura, N.; Suzuki, A. Palladium-Catalyzed Cross-Coupling Reactions of Organoboron Compounds. *Chem. Rev.* **1995**, *95* (7), 2457−2483.
(42) Bennett, T. D.; Cheetham, A. K. Amorphous metal-organic frameworks. *Acc. Chem. Res.* **2014**, *47* (5), 1555−62.
(43) Zhai, Y.; Liu, G.; Jin, F.; Zhang, Y.; Gong, X.; Miao, Z.; Li, J.; Zhang, M.; Cui, Y.; Zhang, L.; et al. Construction of Covalent-Organic Frameworks (COFs) from Amorphous Covalent Organic Polymers via Linkage Replacement. *Angew. Chem., Int. Ed.* **2019**, *58* (49), 17679−17683.
(44) Bennett, T. D.; Goodwin, A. L.; Dove, M. T.; Keen, D. A.; Tucker, M. G.; Barney, E. R.; Soper, A. K.; Bithell, E. G.; Tan, J.-C.; Cheetham, A. K. Structure and properties of an amorphous metal-organic framework. *Phys. Rev. Lett.* **2010**, *104* (11), 115503.
(45) As irresistibly demonstrated on TATHCP-Pd before and after use by the XPS studies, the palladium species incorporated in TATHCP-Pd is $Pd(OAc)_2$ with the Pd in + 2 state. However, the black dots observed in the TEM images of TATHCP-Pd and TATHCP-Pd-reuse (parts d, e, and f of Figure 3), scanning transmission electron (STEM) microscopy images of TATHCP-Pd (Supporting Information), and scanning transmission electron (STEM) microscopy images of TATHCP-Pd-Reuse (Supporting Information) are ascribed to the Pd(0) nanoparticles formed upon the electron-beam induced reduction of the original Pd(II) species during the TEM measurements. This special occasion has formerly been noticed and elucidated by other groups. For example, Wahl et al. observed the formation of palladium nanoparticle arrays from K_2PdCl_4, which was initiated by the electron beam in the TEM. Wahl, R.; Mertig, M.; Raff, J.; Selenska-Pobell, S.; Pompe, W. *Adv. Mater.* **2001**, *13*, 736. Stark et al. found the metalization of $Pd(OAc)_2$ films induced by electron-beam. Stark, T. J.; Mayer, T. M.; Griffis, D. P.; Russell, P. E. J. *J. Vac. Sci. Technol., B: Microelectron. Process. Phenom.* **1991**, *9*, 3475. Stark, T. J.; Mayer, T. M.; Griffis, D. P.; Russell, P. E. J. *J. Vac. Sci. Technol., B: Microelectron. Process. Phenom.* **1992**, *10*, 2685. It was also found by Ding et al. that the black dots were absent in the TEM images of the $Pd(OAc)_2$-free Phen sample, but they showed up in those of the $Pd(OAc)_2$-coordinated Pd/Phen sample and of the pure $Pd(OAc)_2$ sample. Ding, S.-Y.; Gao, J.; Wang, Q.; Zhang, Y.; Song, W.-G.; Su, C.-Y.; Wang, W. *J. Am. Chem. Soc.* **2011**, *133* (49), 19816−19822.
(46) Thomas, A. C. *Photoelectron and Auger Spectroscopy*; Plenum: New York, 1975.
(47) Sing, K. S. W.; Everett, D. H.; Haul, R. A. W.; Moscou, L.; Pierotti, R. A.; Rouquerol, J.; Siemieniewska, T. Reporting physisorption data for gas/solid systems with special reference to the determination of surface area and porosity (Recommendations 1984). *Pure Appl. Chem.* **1985**, *57* (4), 603−19.
(48) Kim, S.; Kim, B.; Dogan, N. A.; Yavuz, C. T. Sustainable Porous Polymer Catalyst for Size-Selective Cross-Coupling Reactions. *ACS Sustainable Chem. Eng.* **2019**, *7* (12), 10865−10872.
(49) Magano, J.; Dunetz, J. R. Large-Scale Applications of Transition Metal-Catalyzed Couplings for the Synthesis of Pharmaceuticals. *Chem. Rev.* **2011**, *111* (3), 2177−2250.

https://dx.doi.org/10.1021/acsaem.0c00539
ACS Appl. Energy Mater. 2020, 3, 4983−4994

(50) Molnár, Á. Efficient, Selective, and Recyclable Palladium Catalysts in Carbon-Carbon Coupling Reactions. *Chem. Rev.* **2011**, *111* (3), 2251−2320.
(51) Ben, T.; Pei, C.; Zhang, D.; Xu, J.; Deng, F.; Jing, X.; Qiu, S. Gas storage in porous aromatic frameworks (PAFs). *Energy Environ. Sci.* **2011**, *4* (10), 3991−3999.
(52) Jeon, H. J.; Choi, J. H.; Lee, Y.; Choi, K. M.; Park, J. H.; Kang, J. K. Highly Selective CO_2-Capturing Polymeric Organic Network Structures. *Adv. Energy Mater.* **2012**, *2* (2), 225−228.
(53) Liebl, M. R.; Senker, J. Microporous Functionalized Triazine-Based Polyimides with High CO_2 Capture Capacity. *Chem. Mater.* **2013**, *25* (6), 970−980.
(54) Jackson, K. T.; Rabbani, M. G.; Reich, T. E.; El-Kaderi, H. M. Synthesis of highly porous borazine-linked polymers and their application to H_2, CO_2, and CH_4 storage. *Polym. Chem.* **2011**, *2* (12), 2775−2777.
(55) Dawson, R.; Adams, D. J.; Cooper, A. I. Chemical tuning of CO_2 sorption in robust nanoporous organic polymers. *Chem. Sci.* **2011**, *2* (6), 1173−1177.
(56) Li, P.-Z.; Zhao, Y. Nitrogen-Rich Porous Adsorbents for CO_2 Capture and Storage. *Chem. - Asian J.* **2013**, *8* (8), 1680−1691.
(57) Qiao, S.; Wei, H.; Wang, T.; Huang, W.; Gu, C.; Yang, R.; Li, X. A ribbon-like ultramicroporous conjugated polycarbazole network for gas storage and separation. *New J. Chem.* **2016**, *40* (4), 3172−3176.
(58) Saleh, M.; Lee, H. M.; Kemp, K. C.; Kim, K. S. Highly stable CO_2/N_2 and CO_2/CH_4 selectivity in hyper-cross-linked heterocyclic porous polymers. *ACS Appl. Mater. Interfaces* **2014**, *6* (10), 7325−33.
(59) Mastalerz, M.; Hauswald, H.-J. S.; Stoll, R. Metal-assisted salphen organic frameworks (MaSOFs) with high surface areas and narrow pore-size distribution. *Chem. Commun.* **2012**, *48* (1), 130−132.
(60) Germain, J.; Svec, F.; Fréchet, J. M. J. Preparation of Size-Selective Nanoporous Polymer Networks of Aromatic Rings: Potential Adsorbents for Hydrogen Storage. *Chem. Mater.* **2008**, *20* (22), 7069−7076.
(61) Katsoulidis, A. P.; Kanatzidis, M. G. Mesoporous Hydrophobic Polymeric Organic Frameworks with Bound Surfactants. Selective Adsorption of C_2H_6 versus CH_4. *Chem. Mater.* **2012**, *24* (3), 471−479.
(62) Rabbani, M. G.; El-Kaderi, H. M. Synthesis and Characterization of Porous Benzimidazole-Linked Polymers and Their Performance in Small Gas Storage and Selective Uptake. *Chem. Mater.* **2012**, *24* (8), 1511−1517.
(63) Rabbani, M. G.; Sekizkardes, A. K.; El-Kadri, O. M.; Kaafarani, B. R.; El-Kaderi, H. M. Pyrene-directed growth of nanoporous benzimidazole-linked nanofibers and their application to selective CO2 capture and separation. *J. Mater. Chem.* **2012**, *22* (48), 25409−25417.
(64) Jiang, J.-X.; Su, F.; Trewin, A.; Wood, C. D.; Niu, H.; Jones, J. T. A.; Khimyak, Y. Z.; Cooper, A. I. Synthetic Control of the Pore Dimension and Surface Area in Conjugated Microporous Polymer and Copolymer Networks. *J. Am. Chem. Soc.* **2008**, *130* (24), 7710−7720.
(65) Myers, A. L.; Prausnitz, J. M. Thermodynamics of mixed-gas adsorption. *AIChE J.* **1965**, *11* (1), 121−127.
(66) Yang, X.; Yu, M.; Zhao, Y.; Zhang, C.; Wang, X.; Jiang, J.-X. Hypercrosslinked microporous polymers based on carbazole for gas storage and separation. *RSC Adv.* **2014**, *4* (105), 61051−61055.
(67) Zhu, Y.; Long, H.; Zhang, W. Imine-Linked Porous Polymer Frameworks with High Small Gas (H_2, CO_2, CH_4, C_2H_2) Uptake and CO2/N2 Selectivity. *Chem. Mater.* **2013**, *25* (9), 1630−1635.
(68) Yang, X.; Yao, S.; Yu, M.; Jiang, J.-X. Synthesis and Gas Adsorption Properties of Tetra-Armed Microporous Organic Polymer Networks Based on Triphenylamine. *Macromol. Rapid Commun.* **2014**, *35* (8), 834−839.
(69) Wang, Z. G.; Liu, X.; Wang, D.; Jin, J. Tröger's base-based copolymers with intrinsic microporosity for CO2 separation and effect of Tröger's base on separation performance. *Polym. Chem.* **2014**, *5* (8), 2793−2800.
(70) Qiao, S.; Du, Z.; Yang, R. Design and synthesis of novel carbazole−spacer−carbazole type conjugated microporous networks for gas storage and separation. *J. Mater. Chem. A* **2014**, *2* (6), 1877−1885.
(71) Zhang, X.; Lu, J.; Zhang, J. Porosity Enhancement of Carbazolic Porous Organic Frameworks Using Dendritic Building Blocks for Gas Storage and Separation. *Chem. Mater.* **2014**, *26* (13), 4023−4029.
(72) Ding, S. Y.; Gao, J.; Wang, Q.; Zhang, Y.; Song, W. G.; Su, C. Y.; Wang, W. Construction of covalent organic framework for catalysis: Pd/COF-LZU1 in Suzuki−Miyaura coupling reaction. *J. Am. Chem. Soc.* **2011**, *133* (49), 19816−22.
(73) Llabrés i Xamena, F. X.; Abad, A.; Corma, A.; Garcia, H. MOFs as catalysts: Activity, reusability and shape-selectivity of a Pd-containing MOF. *J. Catal.* **2007**, *250* (2), 294−298.
(74) Wang, L.; Dong, B.; Ge, R.; Jiang, F.; Xu, J. Fluorene-Based Two-Dimensional Covalent Organic Framework with Thermoelectric Properties through Doping. *ACS Appl. Mater. Interfaces* **2017**, *9* (8), 7108−7114.
(75) Chumakov, Y.; Aksakal, F.; Dimoglo, A.; Ata, A.; Palomares-Sánchez, S. A. First-Principles Study of Thermoelectric Properties of Covalent Organic Frameworks. *J. Electron. Mater.* **2016**, *45* (7), 3445−3452.

https://dx.doi.org/10.1021/acsaem.0c00539
ACS Appl. Energy Mater. 2020, 3, 4983−4994